Electrochemistry

Ultrafast Electron Transfer Kinetics of Graphene Grown by Chemical Vapor Deposition

Ran Chen, Nikoloz Nioradze, Padmanabhan Santhosh, Zhiting Li, Sumedh P. Surwade, Ganesh J. Shenoy, David G. Parobek, Min A. Kim, Haitao Liu, and Shigeru Amemiya*
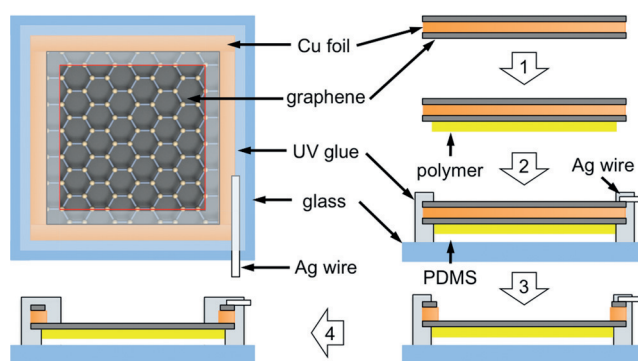
Abstract: High electrochemical reactivity is required for various energy and sensing applications of graphene grown by chemical vapor deposition (CVD). Herein, we report that heterogeneous electron transfer can be remarkably fast at CVD-grown graphene electrodes that are fabricated without using the conventional poly(methyl methacrylate) (PMMA) for graphene transfer from a growth substrate. We use nanogap voltammetry based on scanning electrochemical microscopy to obtain very high standard rate constants $k^0 \geq 25\ cm\,s^{-1}$ for ferrocenemethanol oxidation at polystyrene-supported graphene. The rate constants are at least 2–3 orders of magnitude higher than those at PMMA-transferred graphene, which demonstrates an anomalously weak dependence of electron-transfer rates on the potential. Slow kinetics at PMMA-transferred graphene is attributed to the presence of residual PMMA. This unprecedentedly high reactivity of PMMA-free CVD-grown graphene electrodes is fundamentally and practically important.

Graphene grown by chemical vapor deposition[1] (CVD) is a promising electrode material for various electrochemical applications. There are numerous potential applications of CVD-grown graphene in energy conversion and storage, including in fuel cells, batteries, supercapacitors, and solar cells.[2] The material is also important for electrochemical sensing.[3] The promise of CVD-grown graphene for these electrochemical applications lies in its large area, excellent electrical conductivity, high surface-to-mass ratio, superb transparency, and mechanical robustness and flexibility. In addition, many of these applications require fast electron transfer (ET) between graphene and redox species in a solution. However, it is not fundamentally understood how heterogeneous ET kinetics at graphene/solution interfaces is affected by electronic structure, defects, and impurities.[4]

Currently, the electrochemical reactivity of CVD-grown graphene is considered low in comparison with other sp²-hybridized carbon materials. Electrodes based on CVD-grown monolayer graphene yielded standard ET rate constants, k^0, in a range of 0.01–0.04 cm s⁻¹ for ferrocene-

methanol (FcMeOH)[5] and 0.04–0.2 cm s⁻¹ for (ferrocenyl-methyl)trimethylammonium (FcTMA⁺).[6] These k^0 values for ferrocene-based simple redox couples are 2–3 orders of magnitude lower than those for FcTMA⁺ at single-walled carbon nanotubes (7.6 cm s⁻¹)[7] and highly oriented pyrolytic graphite (HOPG; ≥ 17 cm s⁻¹).[8] Moreover, ET rates at CVD-grown graphene electrodes depended very weakly on the electrode potential to yield anomalously small (< 0.1) or large (> 0.9) transfer coefficients, α, for the reduction or oxidation, respectively, of various redox couples.[5b] In contrast, a normal α value of approximately 0.5 was reported for mechanically exfoliated graphene.[9]

Herein, we demonstrate that the electrochemical reactivity of CVD-grown graphene can be increased by at least 2–3 orders of magnitude compared to that reported in the literature[5] simply by avoiding the conventional use of poly(methyl methacrylate) (PMMA) for electrode fabrication. PMMA has been used almost exclusively to transfer graphene from a metallic growth substrate to a target substrate.[1] During electrode fabrication based on PMMA-mediated transfer, a PMMA film is spread over graphene and is dissolved using organic solvents[5,6] to inevitably leave residual PMMA on the graphene surface.[10] In this work, we assess the effects of PMMA on the electrochemical reactivity of CVD-grown graphene by using polymer-supported electrodes (Scheme 1). With this setup, the graphene surface that is exposed to the redox species is never coated with a PMMA film. In addition, a PMMA-free graphene electrode can be fabricated by using a polystyrene (PS) support. Macroscopic electrodes based on PMMA- and PS-supported graphene

[*] R. Chen, Dr. N. Nioradze, Dr. P. Santhosh, Dr. Z. Li, Dr. S. P. Surwade,
G. J. Shenoy, D. G. Parobek, M. A. Kim, Prof. H. Liu, Prof. S. Amemiya
Department of Chemistry
University of Pittsburgh
219 Parkman Avenue, Pittsburgh, PA 15260 (USA)
E-mail: amemiya@pitt.edu

Scheme 1. Fabrication of a polymer-supported graphene electrode. The method involved 1) drop-casting of a polymer film, 2) attachment of polymer-supported graphene (15×15 mm) to the polydimethylsiloxane (PDMS) support, 3) etching of the Cu foil, and 4) insulation of exposed Cu edges (2–3 mm in length).

yielded reversible cyclic voltammograms (CVs) of the FcMeOH couple at potential sweep rates of up to $0.8\,\mathrm{V\,s^{-1}}$ (see Figure S1 in the Supporting Information). The corresponding k^0 values ($k^0 \geq 0.4\,\mathrm{cm\,s^{-1}}$) for the FcMeOH couple were at least 10–40 times higher than the k^0 values at PMMA-transferred graphene electrodes,[5] which were passivated by residual PMMA.

We employed scanning electrochemical microscopy[11] (SECM) to demonstrate the ultrafast ET kinetics of the FcMeOH couple at polymer-supported graphene electrodes. Specifically, SECM-based nanogap voltammetry[8, 12] was used to investigate both oxidation and reduction of the FcMeOH couple under extremely high mass-transport conditions. In nanogap voltammetry (Figure 1), an ultramicroelectrode with
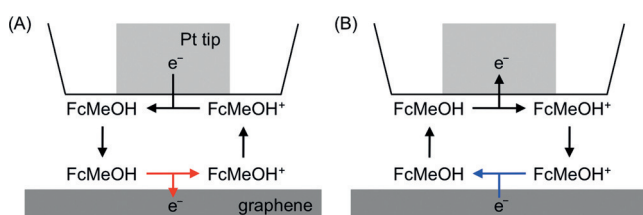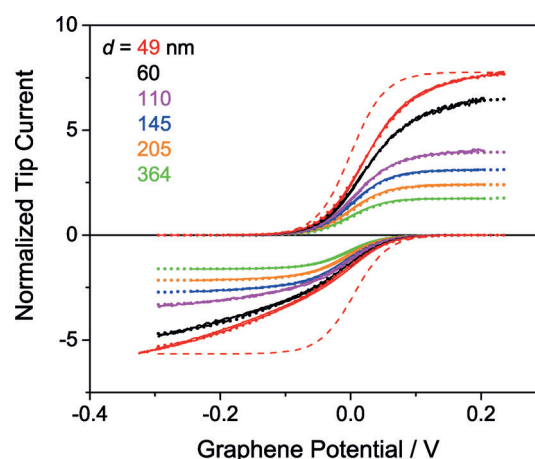
Figure 2. Nanogap voltammograms of 0.5 mM FcMeOH at a PMMA-supported graphene electrode in 1 M KCl (solid lines). The tip currents in the top and bottom panels are based on the SG/TC and feedback modes, respectively. Dotted lines are theoretical curves with $a = 0.49\,\mu\mathrm{m}$, $r_g/a = 2.1$, and employing the parameters given in Table S1. Dashed lines are reversible and were obtained by using the same a and r_g values.

Figure 1. Nanogap voltammetry of the A) oxidation and B) reduction of the FcMeOH couple at a graphene electrode.

a Pt tip radius $a \approx 0.5\,\mu\mathrm{m}$ and a surrounding glass radius $r_g \approx 2a$[12,13] was positioned over the graphene surface to form 30–450 nm-wide nanogaps (Figure S3). The FcMeOH oxidation was voltammetrically driven at the graphene electrode by cycling the electrode potential and was monitored by detecting FcMeOH$^+$ at a diffusion-limited rate at the Pt tip in the substrate-generation/tip-collection (SG/TC) mode (Figure 1 A). Additionally, FcMeOH$^+$ was generated and monitored at a diffusion-limited rate at the tip in order to study the FcMeOH$^+$ reduction at the graphene electrode in the feedback mode (Figure 1 B).

Figure 2 shows nanogap voltammograms of the FcMeOH couple at PMMA-supported graphene electrodes (solid lines). The tip current was normalized against that in the bulk solution ($i_{T,\infty}$; see [Eq. S3] in the Supporting Information). The graphene potential was given against the formal potential of the FcMeOH couple. Each pair of voltammograms shown in the same color was obtained at an identical tip–graphene distance (d) without significant thermal drift in tip position.[14] Each voltammogram was sigmoidal and retractable during a potential cycle as a result of the quasi-steady-state diffusion of redox species across a tip–graphene nanogap.[12]

Nanogap voltammograms of FcMeOH oxidation at PMMA-supported graphene electrodes (Figure 2, upper section) were controlled by heterogeneous ET kinetics. These voltammograms were broader than expected for reversible voltammograms that were limited by the diffusion of FcMeOH across a tip–graphene nanogap (for example, the dashed line at $d = 49$ nm). All voltammograms of FcMeOH oxidation at PMMA-supported graphene electrodes fit very well with theoretical voltammograms with a normal α value

of 0.50 (dotted lines) to yield consistent k^0 values in a range of 1.0–$2.1\,\mathrm{cm\,s^{-1}}$ at various tip–graphene distances (Table S1). Overall, $k^0 = 1.6 \pm 0.5\,\mathrm{cm\,s^{-1}}$ and $\alpha = 0.5$ were obtained at various vertical and lateral tip positions ($N = 37$, where N is the number of tip positions) above six PMMA-supported graphene electrodes. These k^0 values are 25–100 times higher than those at PMMA-transferred graphene electrodes,[5] which were passivated by residual PMMA.

Anomalously, nanogap voltammograms of FcMeOH$^+$ reduction at PMMA-supported graphene electrodes (Figure 2, lower section) were much broader than the kinetically limited voltammograms of FcMeOH oxidation with a normal α value of 0.5 when tip–graphene distances were short (49–110 nm). The feedback tip current did not reach a diffusion-limited value even at very negative potentials. Good fits of experimental voltammograms with theoretical voltammograms yielded significantly low α and k^0 values of 0.29 ± 0.3 and $0.5 \pm 0.2\,\mathrm{cm\,s^{-1}}$ ($N = 23$), respectively. We ascribe this weak potential dependence to a double-layer effect from the positive charges of the PMMA surface based on the oxidative removal of cryptoelectrons by the graphene electrode. Liu and Bard reported that cryptoelectrons of the PMMA surface can be readily removed at much more negative potentials than the formal potential of the FcMeOH couple to reduce redox species in solution.[15] With our setup, the positive charges of the underlying PMMA surface do not affect the access of electrically neutral FcMeOH to graphene (Figure 3 A), thereby yielding an α value of 0.50 for its oxidation. In contrast, access of the positively charged FcMeOH$^+$ to graphene is hampered by the positive surface charges of PMMA (Figure 3 B). Consequently, FcMeOH$^+$ reduction at PMMA-supported graphene electrodes requires a more negative potential, thus yielding a smaller α value of circa 0.3.

We employed SECM-based nanogap voltammetry to find that the ET kinetics of the FcMeOH couple at PMMA-free,
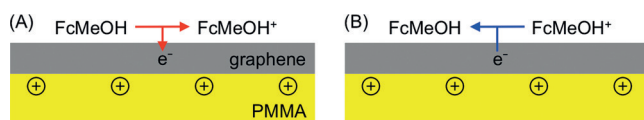
Figure 3. Double-layer effects on A) oxidation and B) reduction of the FcMeOH couple at PMMA-supported graphene electrodes.
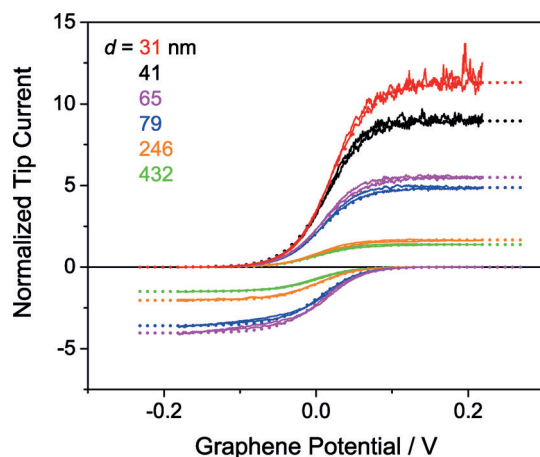

Figure 4. Nanogap voltammograms of 0.5 mM FcMeOH at PS-supported graphene in 1 M KCl (solid lines). The tip currents in the top and bottom panels are based on SG/TC and feedback modes, respectively. Dotted lines are the reversible voltammograms calculated with $a = 0.49$ μm, $r_g/a = 1.7$, and the parameters given in Table S2.

PS-supported graphene electrodes are unprecedentedly fast. Reversible nanogap voltammograms (see Figure 4 for an example) were obtained at PS-supported graphene ($N = 32$ for three electrodes). From the voltammograms, extremely high k^0 values ($k^0 \geq 25$ cm s^{-1}) were calculated as the tip approached the graphene surface to a distance of 31 nm (Table S2; Figure S4). These k^0 values are similar to the k^0 values for FcTMA$^+$ at HOPG (≥ 17 cm s^{-1}).[8] This similarity suggests that the electrochemical reactivity of graphene as the top layer of HOPG is very different from that of graphene on a polar and positively charged PMMA support and is more analogous to that of graphene on a nonpolar and neutral PS support. Noticeably, cryptoelectrons were not removable from the surface of PS nanospheres around the formal potential of the FcMeOH couple.[16] Mechanistically, the slower ET kinetics of PMMA-supported graphene is ascribed to the weakened electronic coupling of graphene with the FcMeOH couple or its hampered reorganization at the interface by the positive charges and dipoles of the PMMA surface. Interestingly, k^0 values for the FcMeOH couple at PS-supported graphene were much higher than the k^0 values of 0.5 ± 0.1 cm s^{-1} at PMMA-transferred graphene with a high defect density,[5c] which were introduced by Ar$^+$ irradiation to electronically activate graphene. Much higher k^0 values at PS-supported graphene indicate that the electrochemical reactivity of Ar$^+$-irradiated graphene was limited by the presence of residual PMMA.

Importantly, nanogap voltammograms of FcMeOH$^+$ reduction at PS-supported graphene electrodes quickly reached limiting currents without the feature of weak potential dependence (Figure 4, lower section). This result supports the idea that PMMA caused an anomalously weak potential dependence for FcMeOH$^+$ reduction in this and in previous[5b] studies. Noticeably, limiting currents during FcMeOH$^+$ reduction were much lower than those during FcMeOH oxidation at identical tip positions and were nearly unchanged at tip–graphene distances of less than 50 nm (Figure S5). The asymmetric limiting currents are ascribed to the contamination of the graphene surface with airborne hydrocarbons as confirmed by ATR-FTIR spectra (ATR = attenuated total reflection).[17] The hydrophobic contaminant layer is less permeable to the more hydrophilic FcMeOH$^+$.[8] Accordingly, FcMeOH$^+$ reduction at contaminated graphene was more hindered, yielding a lower limiting current. Importantly, hydrophobic FcMeOH can permeate quickly through the hydrophobic contaminant layer to reveal the ultrafast ET kinetics of PS-supported graphene. In contrast, the apparently much slower ET kinetics of the [Fe(CN)$_6$]$^{4-/3-}$ couple at polymer-supported graphene was limited by the low permeability of the hydrophobic contaminant layer to this multiply charged hydrophilic redox couple (Figure S6).

In conclusion, the electrochemical reactivity of PS-supported CVD-grown graphene to the FcMeOH redox couple is at least 2–3 orders of magnitude higher than that of PMMA-transferred graphene.[5] Remarkably, the k^0 values at PMMA-free graphene (≥ 25 cm s^{-1}) exceeded the highest k^0 value reported to date for the FcMeOH couple, which is 6.8 cm s^{-1} at Pt nanoelectrodes.[18] The unprecedentedly high electrochemical reactivity of CVD-grown graphene is highly significant both fundamentally and practically. Additionally, this work demonstrates the electrochemical transparency of atomically thin graphene, where a supporting material can affect ET kinetics. The hydrophobic airborne contamination of graphene[17] must be prevented to reliably study the electrochemical reactivity of graphene not only to outer-sphere redox couples,[9,19] which are typically multiply charged and hydrophilic,[5b] but also to inner-sphere redox couples, which are surface sensitive.[4]

Experimental Section

Monolayer graphene was grown on a copper foil by the CVD method.[17a] Graphene was coated with a polymer film by drop-casting a chlorobenzene solution of 46 mg mL^{-1} PMMA or 50 mg mL^{-1} PS. The polymer/graphene/copper/graphene composite was placed over a PDMS support and attached to a glass plate using UV-cure glue. The copper foil was etched in 0.2 M ammonium persulfate for 1.5–2 h or in 1 M FeCl$_3$ in 10% HCl for 40 min to yield polymer-supported graphene. The exposed edges of the copper foil were quickly insulated using UV-cure glue to minimize the airborne contamination of the graphene surface. The insulated graphene electrode was immersed immediately into ultrapure water with extremely low concentrations of organic impurities for characterization by cyclic voltammetry and SECM.

Acknowledgements

[1] X. S. Li, W. W. Cai, J. H. An, S. Kim, J. Nah, D. X. Yang, R. Piner, A. Velamakanni, I. Jung, E. Tutuc, S. K. Banerjee, L. Colombo, R. S. Ruoff, *Science* **2009**, *324*, 1312.

[2] F. Bonaccorso, L. Colombo, G. Yu, M. Stoller, V. Tozzini, A. C. Ferrari, R. S. Ruoff, V. Pellegrini, *Science* **2015**, *347*, 1246501.

[3] W. Yang, K. R. Ratinac, S. P. Ringer, P. Thordarson, J. J. Gooding, F. Braet, *Angew. Chem. Int. Ed.* **2010**, *49*, 2114; *Angew. Chem.* **2010**, *122*, 2160.

[4] R. L. McCreery, M. T. McDermott, *Anal. Chem.* **2012**, *84*, 2602.

[5] a) W. Li, C. Tan, M. A. Lowe, H. D. Abruña, D. C. Ralph, *ACS Nano* **2011**, *5*, 2264; b) N. L. Ritzert, J. Rodriguez-López, C. Tan, H. D. Abruña, *Langmuir* **2013**, *29*, 1683; c) J.-H. Zhong, J. Zhang, X. Jin, J.-Y. Liu, Q. Li, M.-H. Li, W. Cai, D.-Y. Wu, D. Zhan, B. Ren, *J. Am. Chem. Soc.* **2014**, *136*, 16609.

[6] A. G. Güell, N. Ebejer, M. E. Snowden, J. V. Macpherson, P. R. Unwin, *J. Am. Chem. Soc.* **2012**, *134*, 7258.

[7] I. Heller, J. Kong, H. A. Heering, K. A. Williams, S. G. Lemay, C. Dekker, *Nano Lett.* **2005**, *5*, 137.

[8] N. Nioradze, R. Chen, N. Kurapati, A. Khvataeva-Domanov, S. Mabic, S. Amemiya, *Anal. Chem.* **2015**, *87*, 4836.

[9] M. Velický, D. F. Bradley, A. J. Cooper, E. W. Hill, I. A. Kinloch, A. Mishchenko, K. S. Novoselov, H. V. Patten, P. S. Toth, A. T. Valota, S. D. Worrall, R. A. W. Dryfe, *ACS Nano* **2014**, *8*, 10089.

[10] A. Pirkle, J. Chan, A. Venugopal, D. Hinojos, C. W. Magnuson, S. McDonnell, L. Colombo, E. M. Vogel, R. S. Ruoff, R. M. Wallace, *Appl. Phys. Lett.* **2011**, *99*, 122108.

[11] S. Amemiya, A. J. Bard, F.-R. F. Fan, M. V. Mirkin, P. R. Unwin, *Annu. Rev. Anal. Chem.* **2008**, *1*, 95.

[12] N. Nioradze, J. Kim, S. Amemiya, *Anal. Chem.* **2011**, *83*, 828.

[13] J. Kim, A. Izadyar, N. Nioradze, S. Amemiya, *J. Am. Chem. Soc.* **2013**, *135*, 2321.

[14] J. Kim, M. Shen, N. Nioradze, S. Amemiya, *Anal. Chem.* **2012**, *84*, 3489.

[15] C.-Y. Liu, A. J. Bard, *J. Am. Chem. Soc.* **2009**, *131*, 6397.

[16] T. S. Varleý, M. Rosillo-Lopez, S. Sehmi, N. Hollingsworth, K. B. Holt, *Phys. Chem. Chem. Phys.* **2015**, *17*, 1837.

[17] a) Z. Li, Y. Wang, A. Kozbial, G. Shenoy, F. Zhou, R. McGinley, P. Ireland, B. Morganstein, A. Kunkel, S. P. Surwade, L. Li, H. Liu, *Nat. Mater.* **2013**, *12*, 925; b) A. Kozbial, Z. Li, C. Conaway, R. McGinley, S. Dhingra, V. Vahdat, F. Zhou, B. D'Urso, H. Liu, L. Li, *Langmuir* **2014**, *30*, 8598.

[18] P. Sun, M. V. Mirkin, *Anal. Chem.* **2006**, *78*, 6526.

[19] M. Velický, M. A. Bissett, P. S. Toth, H. V. Patten, S. D. Worrall, A. N. J. Rodgers, E. W. Hill, I. A. Kinloch, K. S. Novoselov, T. Georgiou, L. Britnell, R. A. W. Dryfe, *Phys. Chem. Chem. Phys.* **2015**, *17*, 17844.